Compressive Sampling for Scattering Data Collection in Microwave Imaging

G. Oliveri, N. Anselmi, M. Salucci, L. Poli, and A. Massa

2024/09/13

Contents

1 Numerical Results, Part #2: Retrieval of Non-Aggregated Pixels

Numerical results, Part #2: Retrieval of the Contrast Profile via ℓ_1-Minimization

1.1 ℓ_1 Parameters Calibration

OBJECTIVE: This Sub-Section is aimed at calibrating the input parameter of the ℓ_1-Magic solver used to solve the following problem:

$$\begin{aligned} &\min \left\|\mathbf{J}_{eq}^{v}\right\|_1 \\ &subject\ to\ \left\|\mathbf{E}_{scatt}^{v}-\mathbf{G}\mathbf{J}_{eq}^{v}\right\|_2 \leq \eta \end{aligned} . \tag{1}$$

The parameter η control the matching with the data: since it depends on the number of sampling points M, an auxiliary parameter γ_{init} will be calibrated. Then, the parameter η will be find according to:

$$\eta = \gamma_{init} \left\|\mathbf{E}_{scatt}^{v}\right\|_2 \tag{2}$$

The data matching parameter is also analyzed in the following, which is defined as

$$\chi = \left\|\mathbf{E}_{scatt}^{v}-\mathbf{G}\mathbf{J}_{eq}^{v}\right\|_2 \tag{3}$$

Test Case Description

Direct solver:

- Side of the investigation domain: $L = 3.0\lambda$
- Cubic domain divided in $\sqrt{D} \times \sqrt{D}$ cells
- Number of cells for the direct solver: $D = 1600$ (discretization $= \lambda/10$)

Investigation domain:

- Cubic domain divided in $\sqrt{N} \times \sqrt{N}$ cells
- Number of cells for the inversion: $N = 324$

Measurement domain:

- Total number of measurements: $M \in [2 : 38]$
- Measurement points placed on circles of radius $\rho = 3.0\lambda$

Sources:

- Plane waves

- Number of views: $V = 1$; $\theta_{inc}^{v} = 0^{\circ}$
- Amplitude: $A = 1.0$
- Frequency: $F = 300$ MHz ($\lambda = 1$)

Background:

- $\varepsilon_r = 1.0$
- $\sigma = 0$ [S/m]
- Scatterers size/sparsity factor: $S = 1$

1.1.1 Calibration of γ_{init} - $S = 1$

Original Profile

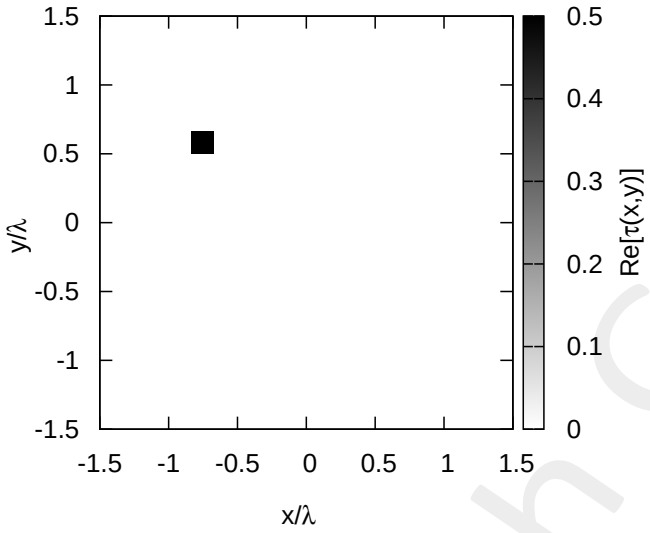

Figure 1: (a) Actual profile.

Average Reconstruction Errors vs. γ_{init}

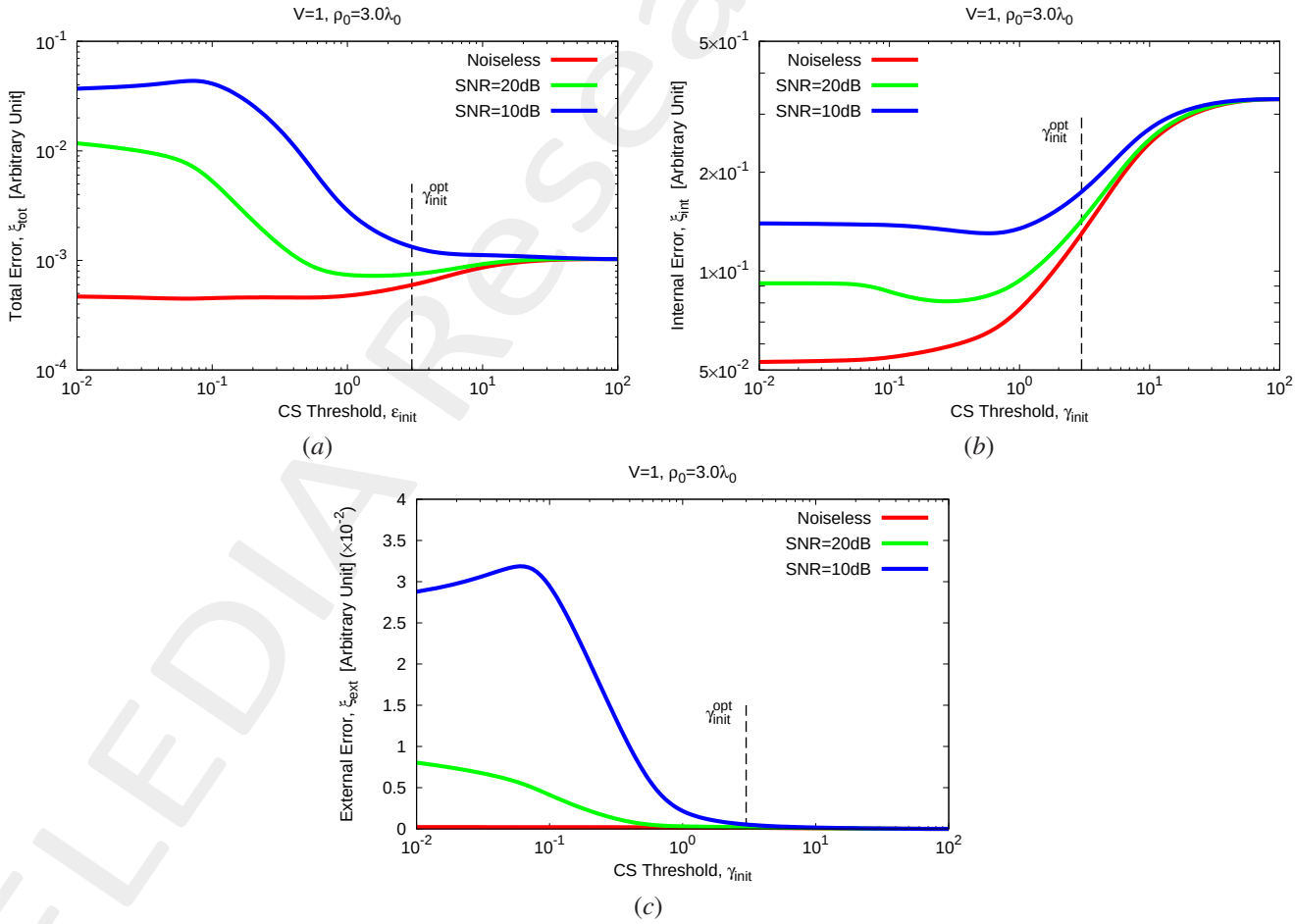

Figure 2: (a) Total, (b) internal and (c) external average reconstruction errors.

OUTCOMES:

- The optimal parameter γ_{init} has been found to be $\gamma_{init} = 3.0$ through the calibration process.

Reconstruction Errors and Data Matching vs. γ_{init} and M

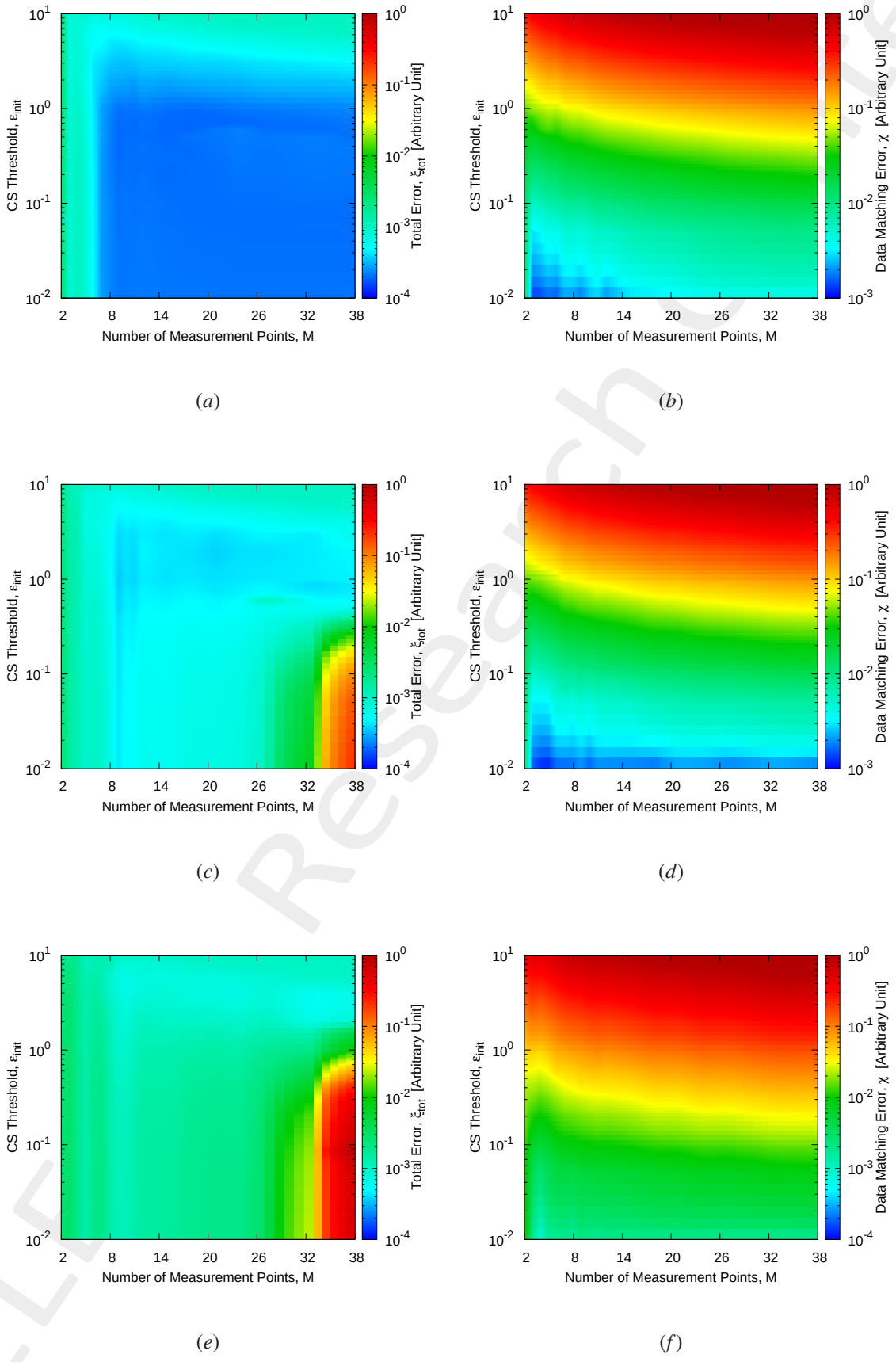

Figure 3: $(a)(c)(e)$ Total reconstruction error and $(b)(d)(f)$ data matching error as a function of M and γ_{init} considering $(a)(b)$ Noiseless case, $(c)(d) SNR = 20$ [dB] and $(e)(f)$ $SNR = 10$ [dB].

OUTCOMES:

Figures 3(*c*) and 3(*e*) show that for noisy cases and number of measurement points higher than $M > 27$ the results are affected by the overfitting phenomenon (i.e., the matching error is low but the reconstruction error is high since the solution found is corrupted by the presence of noise on the matched data).

1.2 Preliminary Result - $S = 1$, Single Pixel

OBJECTIVE: This Section is aimed to validate the proposed approach through a preliminary test case in which a simple single-pixel object is reconstructed. The performance in terms of reconstruction accuracy are evaluated in a comparative fashion with the results obtained obtained when using a *uniform* measurement setup.

Test Case Description

Direct solver:

- Side of the investigation domain: $L = 3.0\lambda$
- Cubic domain divided in $\sqrt{D} \times \sqrt{D}$ cells
- Number of cells for the direct solver: $D = 1600$ (discretization $= \lambda/10$)

Investigation domain:

- Cubic domain divided in $\sqrt{N} \times \sqrt{N}$ cells
- Number of cells for the inversion: $N = 324$

Measurement domain:

- Total number of measurements: $M \in [2 : 38]$
- Measurement points placed on circles of radius $\rho = 3.0\lambda$

Sources:

- Plane waves
- Number of views: $V = 1$; $\theta^v_{inc} = 0°$
- Amplitude: $A = 1.0$
- Frequency: $F = 300$ MHz ($\lambda = 1$)

Background:

- $\varepsilon_r = 1.0$
- $\sigma = 0$ [S/m]

Scatterer:

- Scatterers size/sparsity factor: $S = 1$
- Contrast: $\tau = 0.5$

1.2.1 $S = 1$, $SNR = 20$ **[dB]**

Reconstructed Profiles

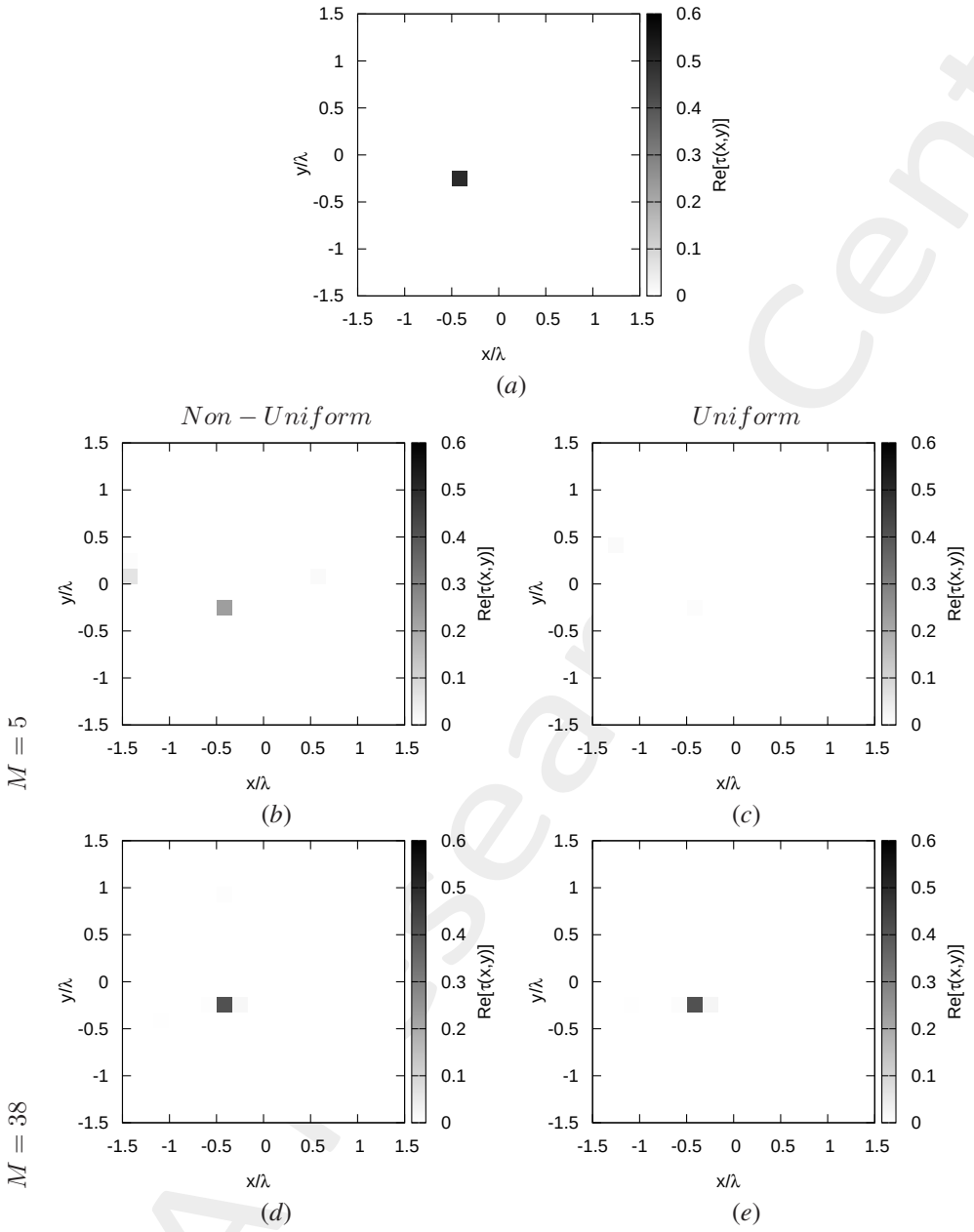

Figure 4: (*a*) Actual and (*b*)-(*e*) reconstructed profiles considering non-uniform optimized and uniform measurement setup.

Resume Error Figures - Total, Internal and External Errors vs. M

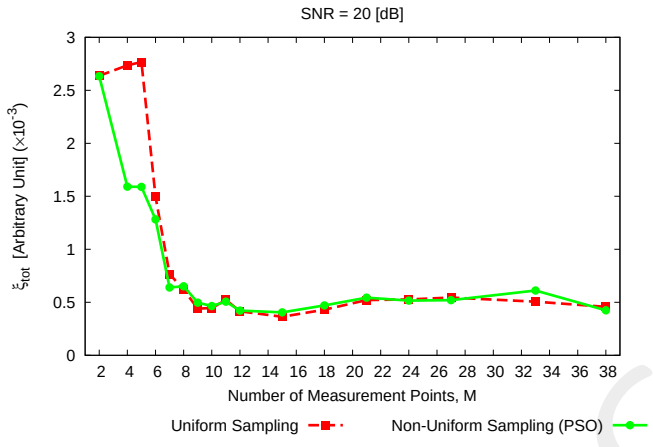

(*a*)

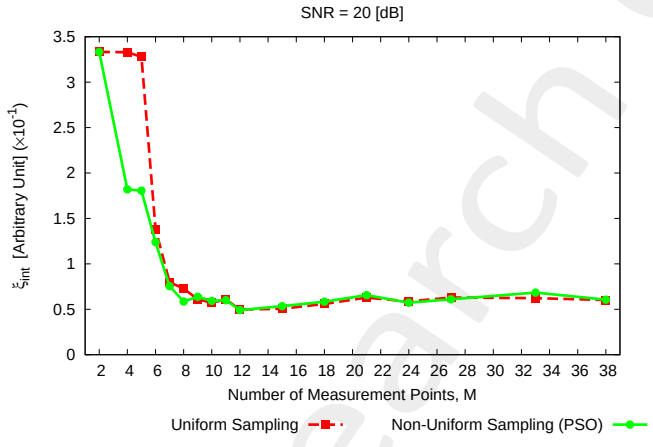

(*b*)

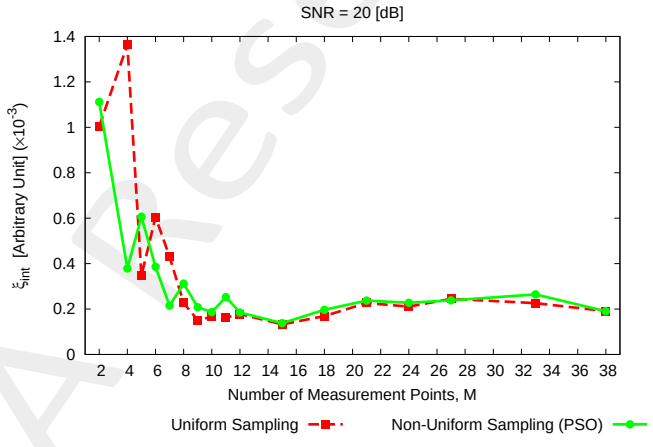

(*c*)

Figure 5: (*a*) Total, (*b*) internal and (*c*) external reconstruction errors vs. number of measurement points M shown in a comparative fashion with those obtained when using a *uniform* measurement setup.

1.3 Retrieval of Non-Aggregated Pixels

OBJECTIVE: This Section is aimed to validate the proposed approach when considering multiple non-adjacent/non-aggregated single-pixel scatterers. The performance in terms of reconstruction accuracy are still evaluated in a comparative fashion with the results obtained obtained when using a *uniform* measurement setup.

Test Case Description

Direct solver:

- Side of the investigation domain: $L = 3.0\lambda$
- Cubic domain divided in $\sqrt{D} \times \sqrt{D}$ cells
- Number of cells for the direct solver: $D = 1600$ (discretization $= \lambda/10$)

Investigation domain:

- Cubic domain divided in $\sqrt{N} \times \sqrt{N}$ cells
- Number of cells for the inversion: $N = 324$

Measurement domain:

- Total number of measurements: $M \in [2 : 38]$
- Measurement points placed on circles of radius $\rho = 3.0\lambda$

Sources:

- Plane waves
- Number of views: $V = 1$; $\theta_{inc}^{v} = 0^{\circ}$
- Amplitude: $A = 1.0$
- Frequency: $F = 300$ MHz ($\lambda = 1$)

Background:

- $\varepsilon_r = 1.0$
- $\sigma = 0$ [S/m]

Scatterer:

- Scatterers size/sparsity factor: $S = 1, 2, 3, 4$
- Contrast: $\tau = 0.5$

1.3.1 Non-Aggregated Pixels, $S = 2$, $SNR = 20$ [dB]

Reconstructed Profiles

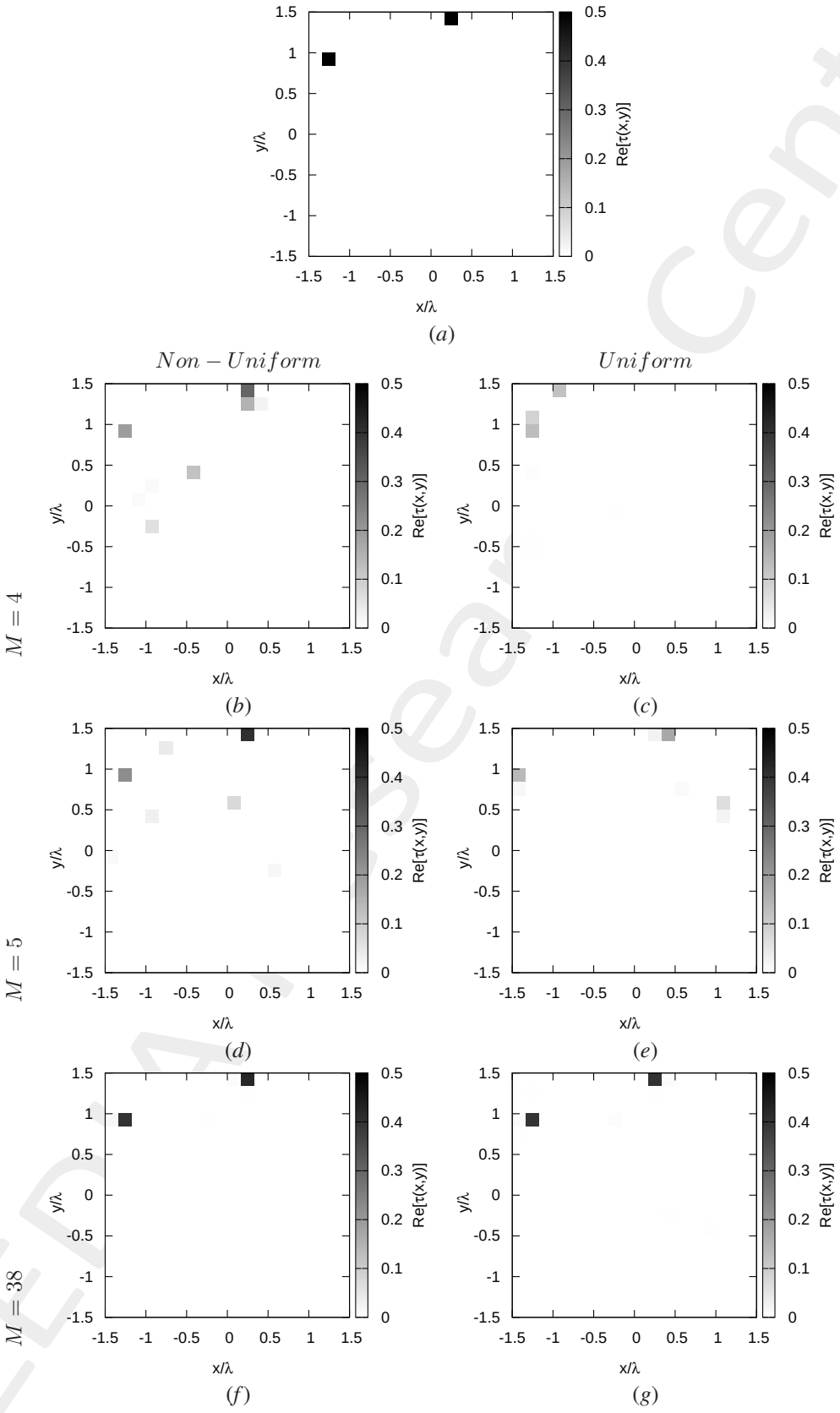

Figure 6: (*a*) Actual and (*b*)(*c*) reconstructed profiles considering (*b*)(*d*)(*f*) non-uniform optimized and (*c*)(*e*)(*g*) uniform measurement setup with (*b*)(*c*) minimum, (*d*)(*e*) intermediate/best and (*f*)(*g*) maximum M.

1.3.2 Non-Aggregated Pixels, $S = 2$, $SNR = 10$ [dB]

Reconstructed Profiles

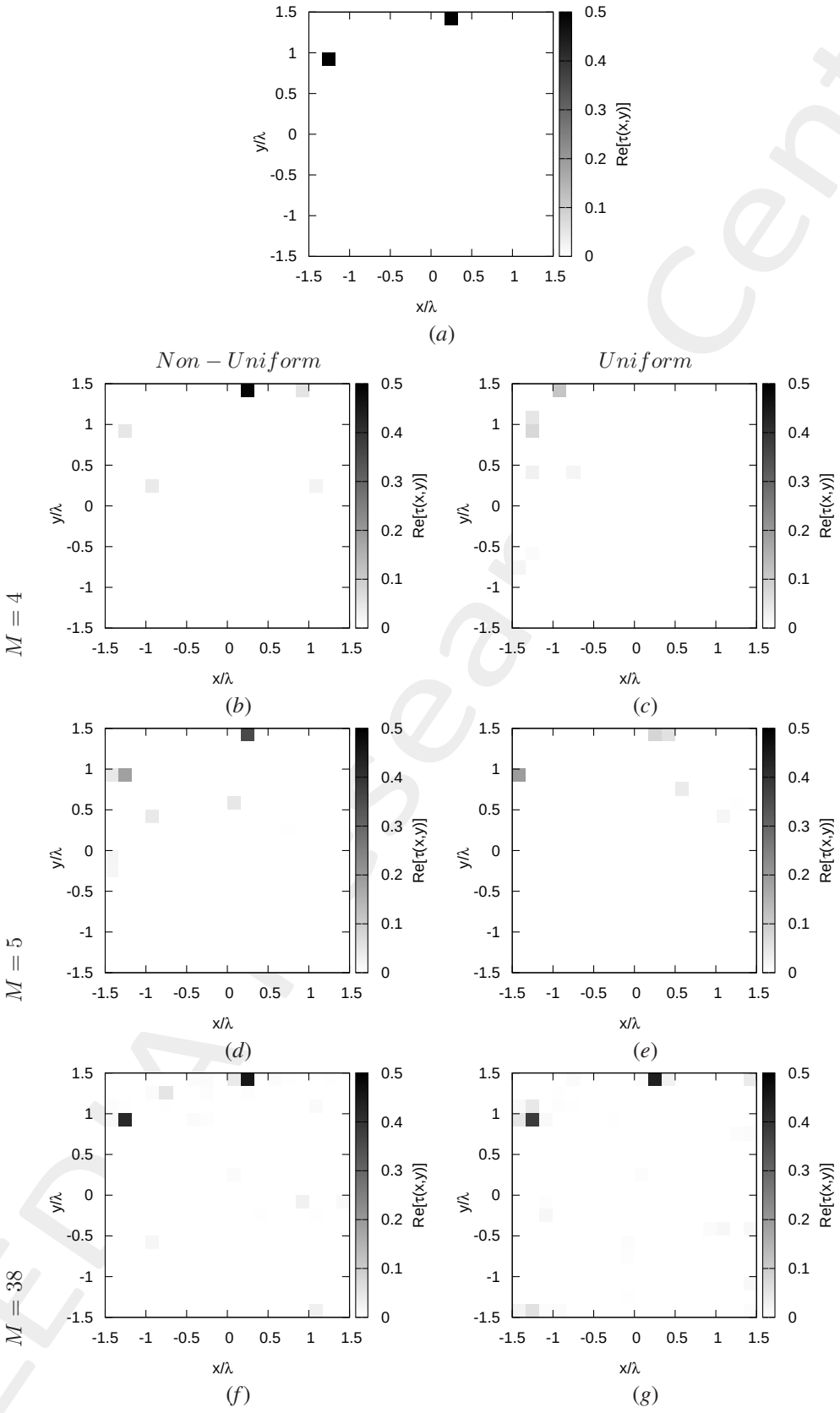

Figure 7: (*a*) Actual and (*b*)(*c*) reconstructed profiles considering (*b*)(*d*)(*f*) non-uniform optimized and (*c*)(*e*)(*g*) uniform measurement setup with (*b*)(*c*) minimum, (*d*)(*e*) intermediate/best and (*f*)(*g*) maximum M.

1.3.3 Non-Aggregated Pixels, $S = 3$, $SNR = 10$ [dB]

Reconstructed Profiles

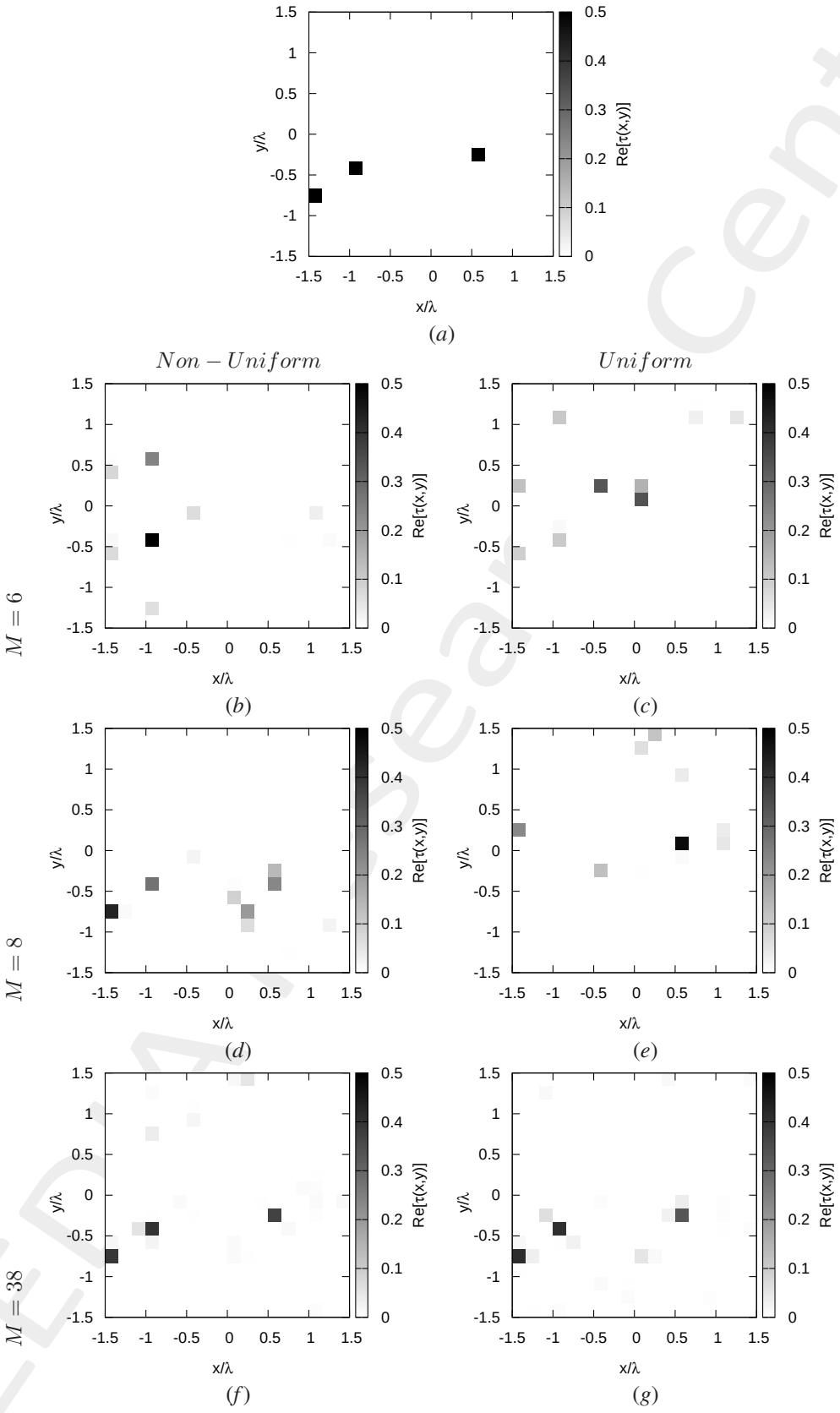

Figure 8: (a) Actual and $(b)(c)$ reconstructed profiles considering $(b)(d)(f)$ non-uniform optimized and $(c)(e)(g)$ uniform measurement setup with $(b)(c)$ minimum, $(d)(e)$ intermediate/best and $(f)(g)$ maximum M.

Resume Error Figures - Total, Internal and External Errors vs. M

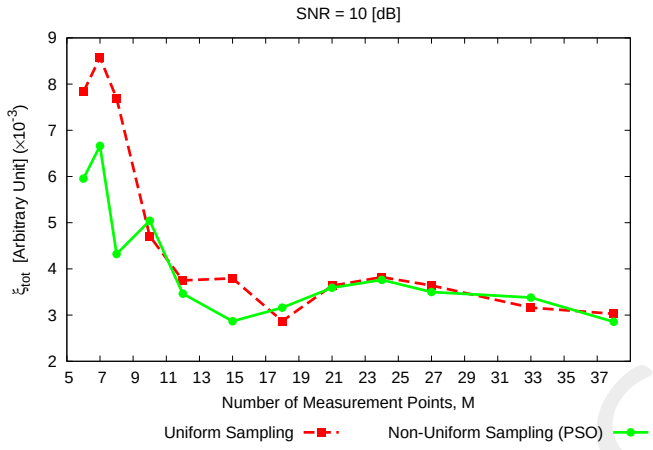

(*a*)

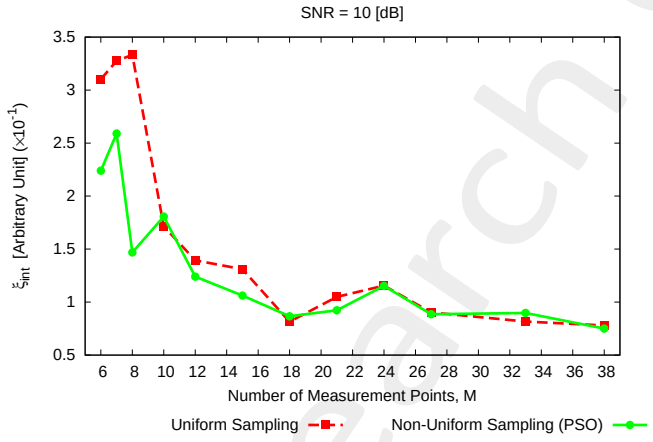

(*b*)

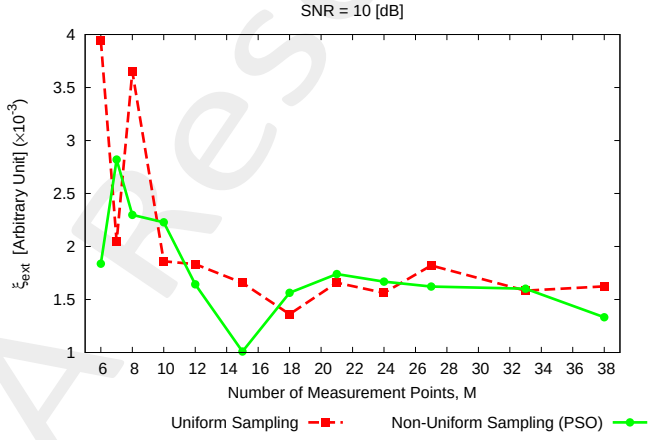

(*c*)

Figure 9: (*a*) Total, (*b*) internal and (*c*) external reconstruction errors vs. number of measurement points M shown in a comparative fashion with those obtained when using a *uniform* measurement setup.

1.3.4 Non-Aggregated Pixels, $S = 4$, $SNR = 20$ [dB]

Reconstructed Profiles

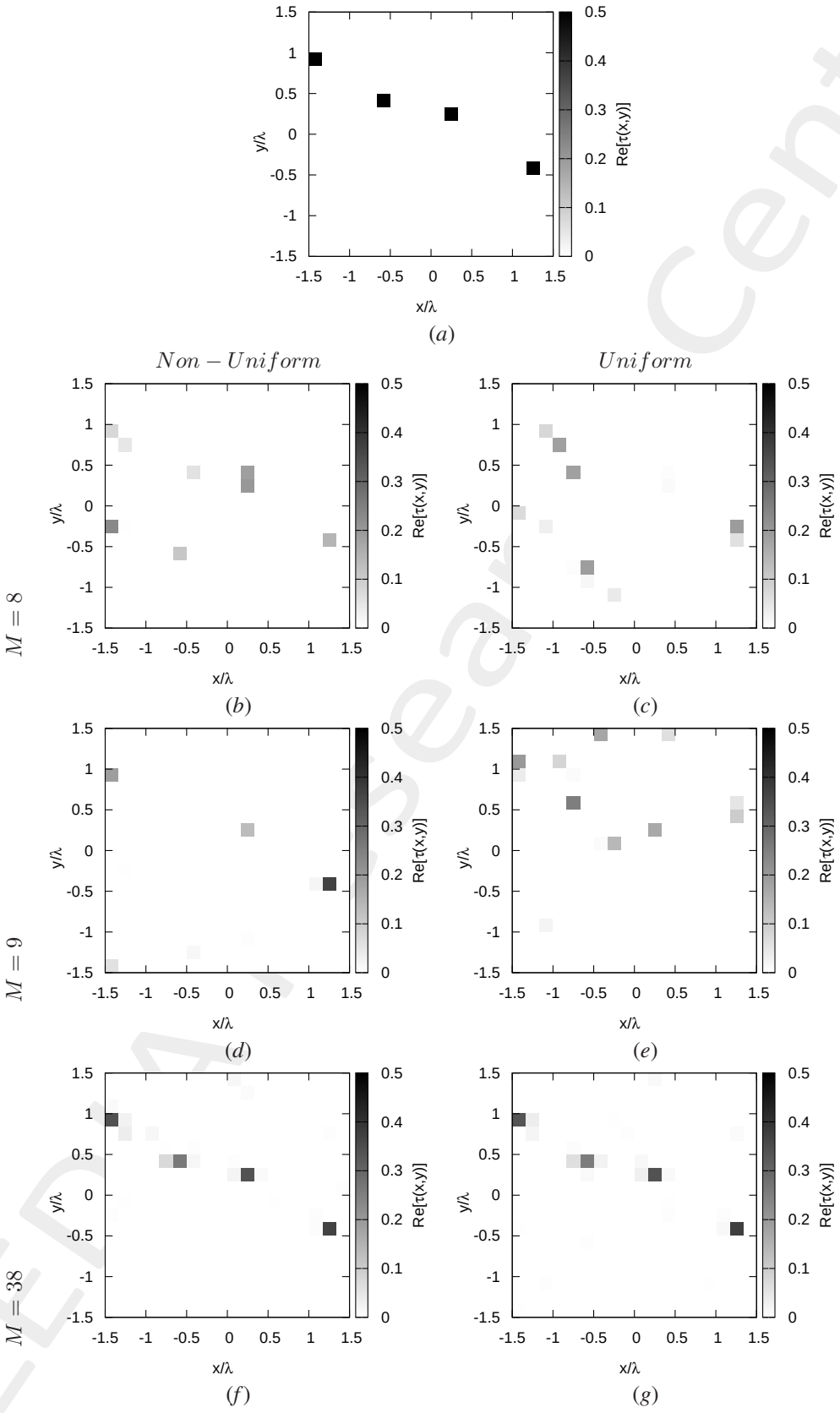

Figure 10: (*a*) Actual and (*b*)(*c*) reconstructed profiles considering (*b*)(*d*)(*f*) non-uniform optimized and (*c*)(*e*)(*g*) uniform measurement setup with (*b*)(*c*) minimum, (*d*)(*e*) intermediate/best and (*f*)(*g*) maximum M.

Resume Error Figures - Total, Internal and External Errors vs. M

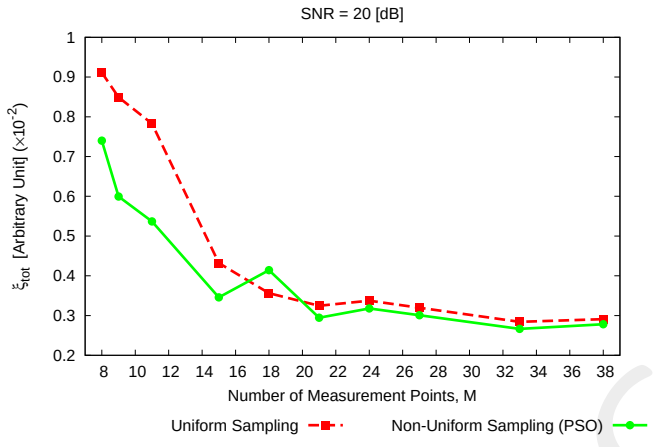

(*a*)

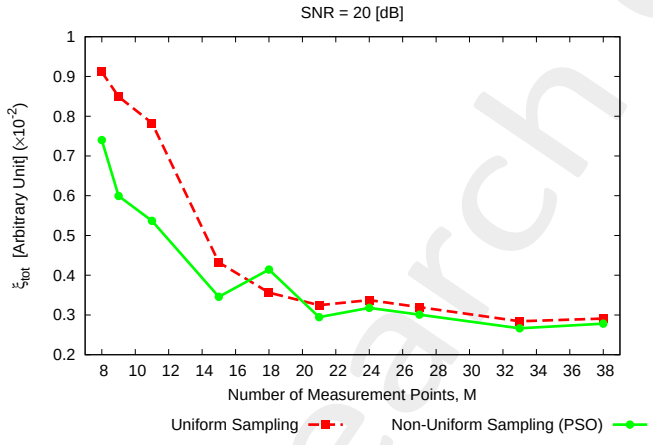

(*b*)

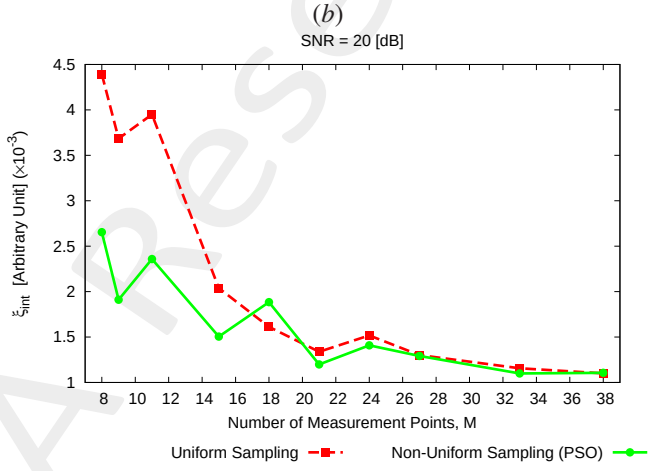

(*c*)

Figure 11: (*a*) Total, (*b*) internal and (*c*) external reconstruction errors vs. number of measurement points M shown in a comparative fashion with those obtained when using a *uniform* measurement setup.

1.3.5 Non-Aggregated Pixels, $S = 5$, $SNR = 20$ [dB]

Reconstructed Profiles

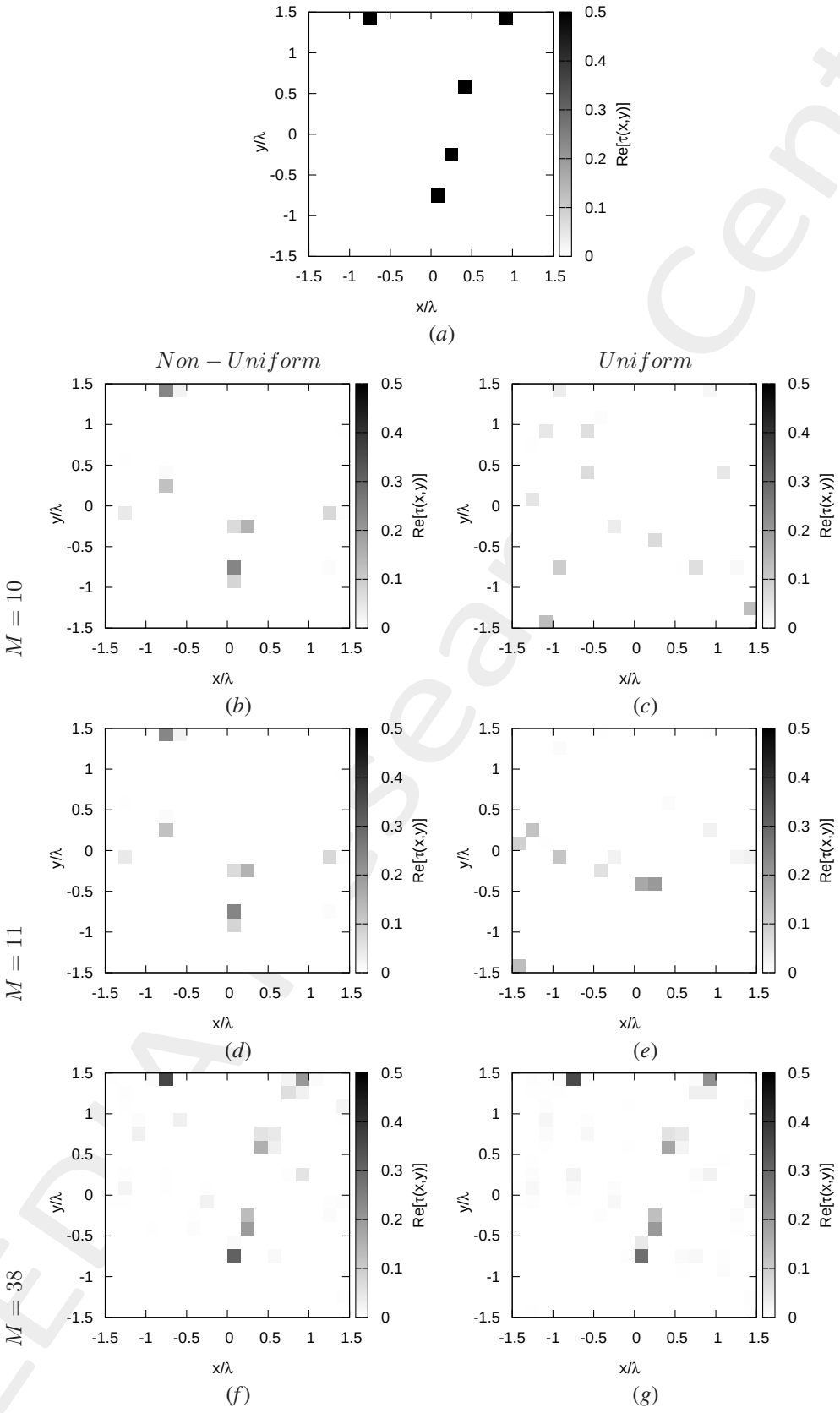

Figure 12: (*a*) Actual and (*b*)(*c*) reconstructed profiles considering (*b*)(*d*)(*f*) non-uniform optimized and (*c*)(*e*)(*g*) uniform measurement setup with (*b*)(*c*) minimum, (*d*)(*e*) intermediate/best and (*f*)(*g*) maximum M.

Resume Error Figures - Total, Internal and External Errors vs. M

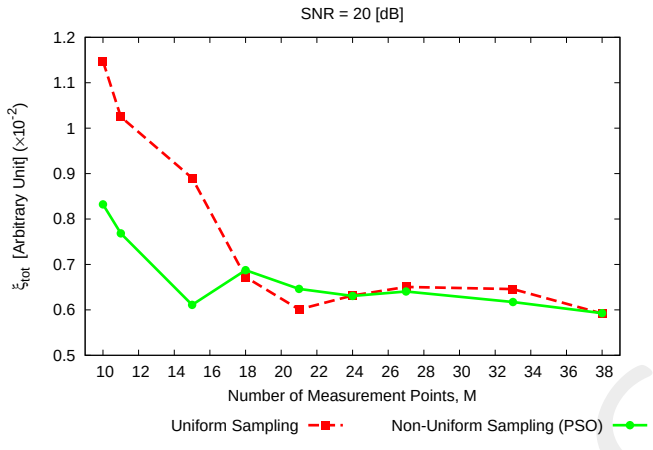

(a)

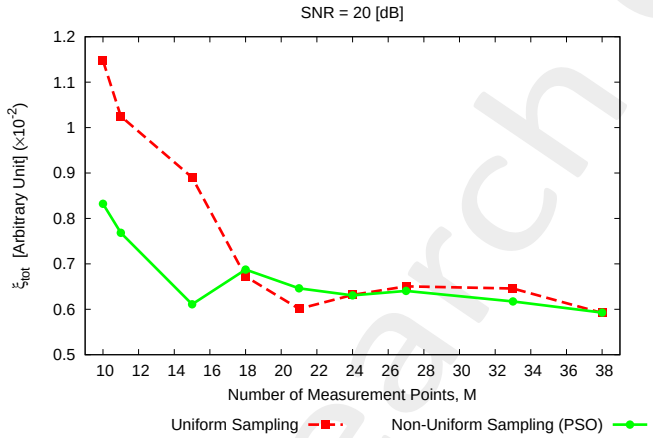

(b)

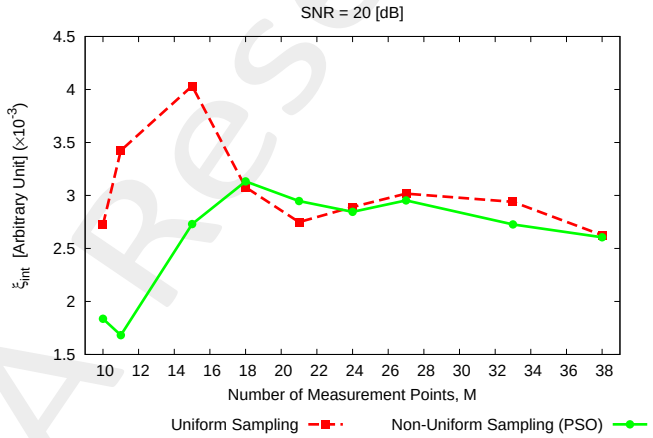

(c)

Figure 13: (a) Total, (b) internal and (c) external reconstruction errors vs. number of measurement points M shown in a comparative fashion with those obtained when using a *uniform* measurement setup.

1.3.6 Non-Aggregated Pixels, $S = 5$, $SNR = 10$ [dB]

Reconstructed Profiles

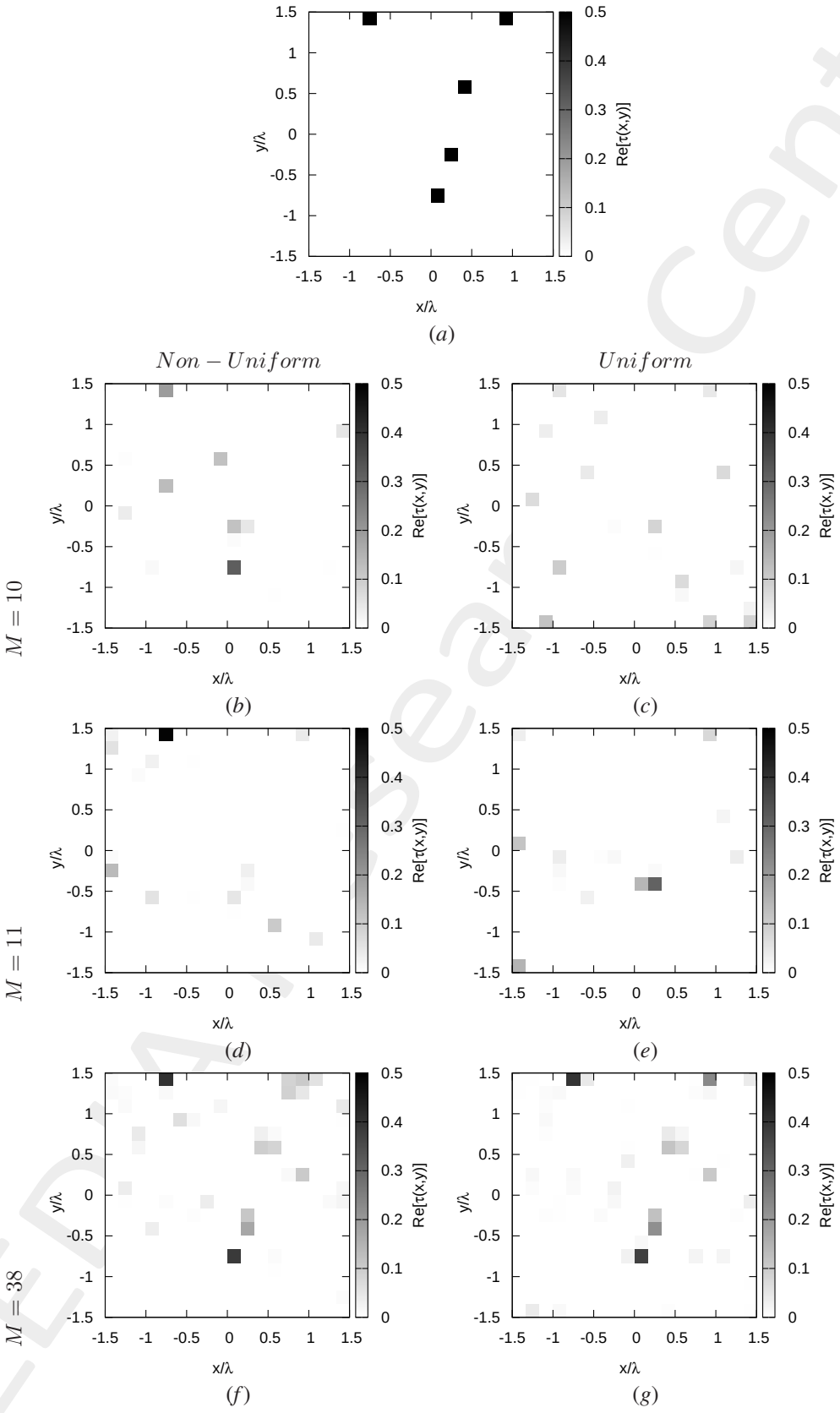

Figure 14: (a) Actual and (b)(c) reconstructed profiles considering (b)(d)(f) non-uniform optimized and (c)(e)(g) uniform measurement setup with (b)(c) minimum, (d)(e) intermediate/best and (f)(g) maximum M.

Resume Error Figures - Total, Internal and External Errors vs. M

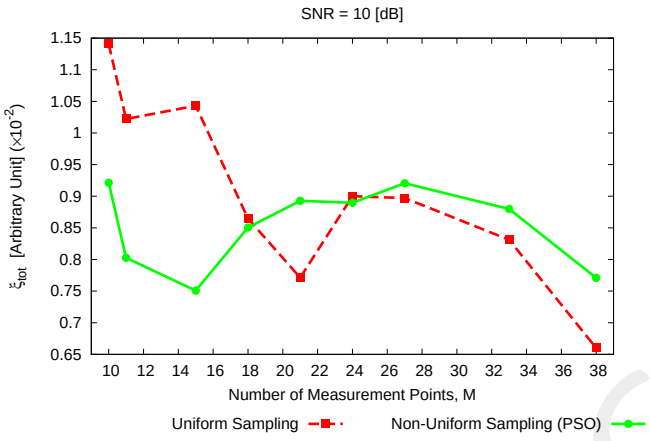

(*a*)

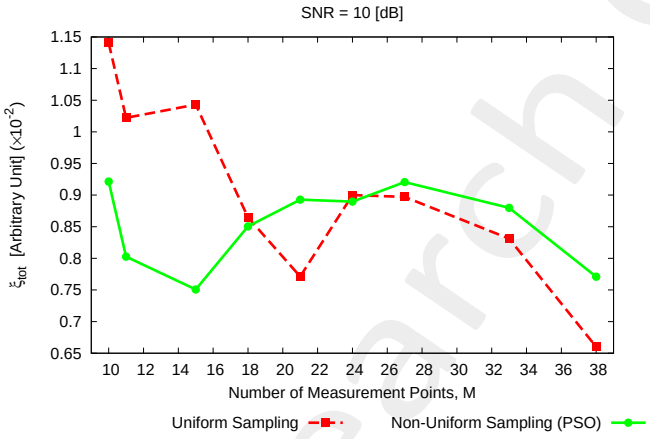

(*b*)

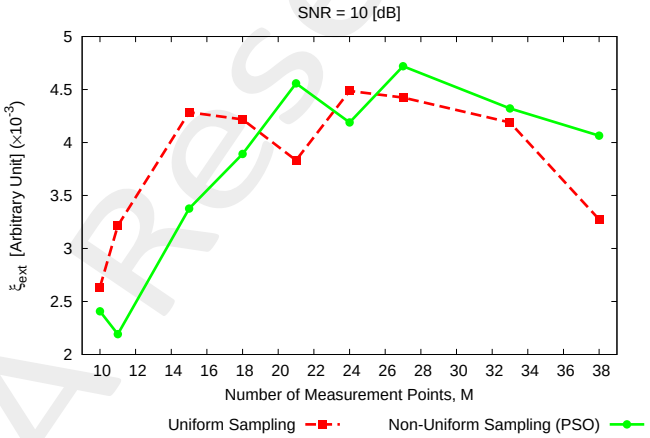

(*c*)

Figure 15: (*a*) Total, (*b*) internal and (*c*) external reconstruction errors vs. number of measurement points M shown in a comparative fashion with those obtained when using a *uniform* measurement setup.

OUTCOMES:

- If the scattered field samples are collected by the sensor placed within the observation domain according to the non-uniform optimized distributions the reconstruction errors are generally lower (or almost equal in some cases) than those obtained considering a conventional uniform distribution (in which the sensor are equally-spaced), whatever

the scatterer distribution. However, sometimes the use of a uniform distribution provides better results (in terms of reconstruction error), but in such cases the reconstruction is not accurate (i.e., the reconstruction fails for both the non-uniform and uniform cases);

- When the number of measurement points approaches the maximum theoretical number necessary to estimate the whole amount of information provided by the scattered field, the reconstruction are generally very similar in both the non-uniform and uniform cases.

More information on the topics of this document can be found in the following list of references.

References

[1] M. Salucci, L. Poli, and G. Oliveri, "Full-vectorial 3D microwave imaging of sparse scatterers through a multi-task Bayesian compressive sensing approach," *Journal of Imaging*, vol. 5, no. 1, pp. 1-24, Jan. 2019.

[2] M. Salucci, A. Gelmini, L. Poli, G. Oliveri, and A. Massa, "Progressive compressive sensing for exploiting frequency-diversity in GPR imaging," *J. Electromagn. Waves Appl. J*, vol. 32, no. 9, pp. 1164-1193, 2018.

[3] G. Oliveri, P.-P. Ding, and L. Poli "3D crack detection in anisotropic layered media through a sparseness-regularized solver,"IEEE Antennas Wireless Propag. Lett., vol. 14, pp. 1031-1034, 2015.

[4] Y. Zhong, F. Zardi, M. Salucci, G. Oliveri, and A. Massa, "Multiscaling differential contraction integral method for inverse scattering problems with inhomogeneous media," *IEEE Trans. Microw. Theory Tech.*, vol. 71, no. 9, pp. 4064-4079, Sep. 2023.

[5] X. Ye, F. Zardi, M. Salucci, and A. Massa, "Multiresolution subspace-based optimization method for the retrieval of 2-D perfect electric conductors," *IEEE Trans. Microw. Theory Tech.*, vol. 71, no. 4, pp. 1732-1744, Apr. 2023.

[6] G. Oliveri, N. Anselmi, M. Salucci, L. Poli, and A. Massa, "Compressive sampling-based scattering data acquisition in microwave imaging," *J. Electromagn. Waves Appl. J*, vol. 37, no. 5, 693-729, Mar. 2023.

[7] M. Salucci, L. Poli, P. Rocca, and A. Massa, "Learned global optimization for inverse scattering problems - Matching global search with computational efficiency," *IEEE Trans. Antennas Propag.*, vol. 70, no. 8, pp. 6240-6255, Aug. 2022.

[8] Y. Zhong, M. Salucci, K. Xu, A. Polo, and A. Massa, "A multi-resolution contraction integral equation method for solving highly non-linear inverse scattering problems," *IEEE Trans. Microw. Theory Tech.*, vol. 68, no. 4, pp. 1234-1247, Apr. 2020.

[9] G. Oliveri, L. Poli, N. Anselmi, M. Salucci, and A. Massa, "Compressive sensing-based Born iterative method for tomographic imaging," *IEEE Tran. Microw. Theory Techn.*, vol. 67, no. 5, pp. 1753-1765, May 2019.

[10] N. Anselmi, L. Poli, G. Oliveri, and A. Massa, "Iterative multi-resolution bayesian CS for microwave imaging," *IEEE Trans. Antennas Propag.*, vol. 66, no. 7, pp. 3665-3677, Jul. 2018.

[11] G. Oliveri, M. Salucci, and N. Anselmi, "Tomographic imaging of sparse low-contrast targets in harsh environments through matrix completion," *IEEE Trans. Microw. Theory Tech.*, vol. 66, no. 6, pp. 2714-2730, Jun. 2018.

[12] G. Oliveri, M. Salucci, N. Anselmi, and A. Massa, "Compressive sensing as applied to inverse problems for imaging: theory, applications, current trends, and open challenges," *IEEE Antennas Propag. Mag.*, vol. 59, no. 5, pp. 34-46, Oct. 2017.

[13] N. Anselmi, G. Oliveri, M. A. Hannan, M. Salucci, and A. Massa, "Color compressive sensing imaging of arbitrary-shaped scatterers," *IEEE Trans. Microw. Theory Techn.*, vol. 65, no. 6, pp. 1986-1999, Jun. 2017.

[14] T. Moriyama, M. Salucci, M. Tanaka, and T. Takenaka, "Image reconstruction from total electric field data with no information on the incident field," *J. Electromagn. Waves Appl. J*, vol. 30, no. 9, pp. 1162-1170, 2016.

[15] N. Anselmi, G. Oliveri, M. Salucci, and A. Massa, "Wavelet-based compressive imaging of sparse targets," *IEEE Trans. Antennas Propag.*, vol. 63, no. 11, pp. 4889-4900, Nov. 2015.

[16] X. Ye, L. Poli, G. Oliveri, Y. Zhong, K. Agarwal, A. Massa, and X. Chen,"Multi-resolution subspace-based optimization method for solving three-dimensional inverse scattering problems," *J. Opt. Soc. America A*, vol. 32, no. 11, pp. 2218-2226, Nov. 2015.

[17] G. Oliveri, N. Anselmi, and A. Massa, "Compressive sensing imaging of non-sparse 2D scatterers by a total-variation approach within the Born approximation," *IEEE Trans. Antennas Propag.*, vol. 62, no. 10, pp. 5157-5170, Oct. 2014.

[18] T. Moriyama, G. Oliveri, M. Salucci, and T. Takenaka, "A multi-scaling forward-backward time-stepping method for microwave imaging," *IEICE Electronics Express*, vol. 11, no. 16, pp. 1-12, Aug. 2014.

[19] L. Poli, G. Oliveri, P.-P. Ding, T. Moriyama, and A. Massa, "Multifrequency Bayesian compressive sensing methods for microwave imaging," *J. Opt. Soc. America A*, vol. 31, no. 11, pp. 2415-2428, 2014.

[20] L. Poli, G. Oliveri, and A. Massa, "Imaging sparse metallic cylinders through a Local Shape Function Bayesian Compressive Sensing approach," *J. Opt. Soc. America A*, vol. 30, no. 6, pp. 1261-1272, 2013.

[21] L. Poli, G. Oliveri, F. Viani, and A. Massa, "MT-BCS-based microwave imaging approach through minimum-norm current expansion," *IEEE Trans. Antennas Propag.*, vol. 61, no. 9, pp. 4722-4732, Sep. 2013.

[22] F. Viani, L. Poli, G. Oliveri, F. Robol, and A. Massa, "Sparse scatterers imaging through approximated multitask compressive sensing strategies," *Microwave Opt. Technol. Lett.*, vol. 55, no. 7, pp. 1553-1558, Jul. 2013.

[23] L. Poli, G. Oliveri, P. Rocca, and A. Massa, "Bayesian compressive sensing approaches for the reconstruction of two-dimensional sparse scatterers under TE illumination," *IEEE Trans. Geosci. Remote Sensing*, vol. 51, no. 5, pp. 2920-2936, May 2013.

[24] L. Poli, G. Oliveri, and A. Massa, "Microwave imaging within the first-order Born approximation by means of the contrast-field Bayesian compressive sensing," *IEEE Trans. Antennas Propag.*, vol. 60, no. 6, pp. 2865-2879, Jun. 2012.

[25] G. Oliveri, A. Randazzo, M. Pastorino, and A. Massa,"Electromagnetic imaging within the contrast-source formulation by means of the multiscaling inexact Newton method," *J. Opt. Soc. America A*, vol. 29, no. 6, pp. 945-958, 2012.

[26] G. Oliveri, L. Poli, P. Rocca, and A. Massa, "Bayesian compressive optical imaging within the Rytov approximation," *Optics Letters*, vol. 37, no. 10, pp. 1760-1762, 2012.

[27] G. Oliveri, P. Rocca, and A. Massa, "A Bayesian compressive sampling-based inversion for imaging sparse scatterers," *IEEE Trans. Geosci. Remote Sensing*, vol. 49, no. 10, pp. 3993-4006, Oct. 2011.

[28] G. Oliveri, Y. Zhong, X. Chen, and A. Massa, "Multi-resolution subspace-based optimization method for inverse scattering," *J. Opt. Soc. America A*, vol. 28, no. 10, pp. 2057-2069, Oct. 2011.

[29] A. Randazzo, G. Oliveri, A. Massa, and M. Pastorino, "Electromagnetic inversion with the multiscaling inexact-Newton method - Experimental validation," *Microwave Opt. Technol. Lett.*, vol. 53, no. 12, pp. 2834-2838, Dec. 2011.

[30] M. Benedetti, D. Lesselier, M. Lambert, and A. Massa, "Multiple shapes reconstruction by means of multi-region level sets," *IEEE Trans. Geosci. Remote Sensing*, vol. 48, no. 5, pp. 2330-2342, May 2010.

[31] M. Benedetti, D. Lesselier, M. Lambert, and A. Massa, "A multi-resolution technique based on shape optimization for the reconstruction of homogeneous dielectric objects," *Inverse Problems*, vol. 25, no. 1, pp. 1-26, Jan. 2009.